Journal of CO2 Utilization 80 (2024) 102668

Contents lists available at ScienceDirect

Journal of CO2 Utilization

journal homepage: www.elsevier.com/locate/jcou

Plasma-based conversion of martian atmosphere into life-sustaining chemicals: The benefits of utilizing martian ambient pressure

Seán Kelly [a,b,*,1], Elizabeth Mercer [a,1], Yury Gorbanev [a], Igor Fedirchyk [a], Claudia Verheyen [a,c], Klaus Werner [d], Pluton Pullumbi [e], Aidan Cowley [f], Annemie Bogaerts [a]

[a] Research group PLASMANT, Department of Chemistry, University of Antwerp, Belgium
[b] School of Electronic Engineering, Dublin City University, Ireland
[c] Chimie des Interactions Plasma-Surface (ChIPS), CIRMAP, Université de Mons, Belgium
[d] pinkRF B.V., Transistorweg 7d, 6534 AT Nijmegen, the Netherlands
[e] Air Liquide, Centre de Recherche Claude-Delorme, Paris-Saclay, France
[f] European Astronaut Centre, European Space Agency, Linder Höhe, D-51147, Germany

ARTICLE INFO

Keywords:
ISRU
Mars
Microwave plasma
Conversion

ABSTRACT

We explored the potential of plasma-based In-Situ Resource Utilization (ISRU) for Mars through the conversion of Martian atmosphere (~96% CO_2, 2% N_2, and 2% Ar) into life-sustaining chemicals. As the Martian surface pressure is about 1% of the Earth's surface pressure, it is an ideal environment for plasma-based gas conversion using microwave reactors. At 1000 W and 10 Ln/min (normal liters per minute), we produced ~76 g/h of O_2 and ~3 g/h of NO_x using a 2.45 GHz waveguided reactor at 25 mbar, which is ~3.5 times Mars ambient pressure. The energy cost required to produce O_2 was ~0.013 kWh/g, which is very promising compared to recently concluded MOXIE experiments on the Mars surface. This marks a crucial step towards realizing the extension of human exploration.

1. Introduction

In February 2021, the Perseverance rover landed on Mars. It was a mission full of firsts, and on April 20th, the Mars OXygen In-Situ resource utilization Experiment (MOXIE) completed its first test in converting Martian atmosphere into product molecules, including O_2 at ~ 98% purity [1]. Using 300 W of power, an atmospheric gas mixture was brought through a Solid OXide Electrolyzer (SOXE) to produce up to 12 g/h of O_2 at peak efficiency [2].

In total, it is estimated that to return four astronauts' home from the Martian surface would require over 25 metric tons (25×10^6 g) of O_2 [3] for rocket propellant, which stresses the importance of technologies like MOXIE. The experiments that MOXIE conducted mark a giant leap forward and show a glimpse of what is possible for utilizing the Martian atmosphere to produce valuable and life-sustaining supplies; however, it is apparent from the sheer magnitude of resources needed for just one mission that the future expansion of human exploration to planets like Mars demands significant improvements or novel technologies to efficiently utilize all of the resources available on the Red Planet.

A recent article by *Engeling et al.* outlined how plasma-based applications could be used for advanced chemical processing in space to support human life during crewed transit and planetary habitation [4]. This study focused on several plasma-based applications being investigated at the National Aeronautics and Space Administration's (NASA) Kennedy Space Center, including plasma waste gasification, plasma-assisted nutrient recovery, hydrogen plasma Lunar regolith reduction, plasma for space agriculture, plasma-activated water, and plasma cleaning and processing [4]. Moreover, the European Space Agency (ESA) has displayed a keen interest in utilizing plasma-based applications and has undertaken several projects aimed at extracting key molecules from Mars' CO_2-rich atmosphere [5]. Although plasma research is still in its early stages (see ***Section: Technological Readiness***), it can potentially influence future planetary colonization strategies. It is clear from the research conducted by both NASA and ESA that plasma-based ISRU is instrumental in advancing space exploration, as well as realizing future human-led missions to Mars.

Microwave (MW) plasma reactors show great potential in an ISRU context. As an emerging technology, MW plasma reactors have

* Corresponding author at: Research group PLASMANT, Department of Chemistry, University of Antwerp, Belgium.
E-mail address: sean.kelly@dcu.ie (S. Kelly).
[1] Authors are co-first authors.

https://doi.org/10.1016/j.jcou.2024.102668
Received 27 October 2023; Received in revised form 27 November 2023; Accepted 3 January 2024
Available online 9 January 2024

demonstrated favorable energy efficiencies and gas conversion at low-sub-atmospheric pressures, such as those found on the surface of Mars, and many studies have reported encouraging results [6–12]; however, few have applied this technology in a Mars ISRU context [5,13,14]. It has been demonstrated that microwave (MW) plasma conversion can produce valuable resources like propellants, oxygen for habitats, and fixed nitrogen for agriculture at a low energy cost, making it an excellent candidate for local generation [5,13], [15]. In our previous study, when using MW plasma at sub-atmospheric pressures (i.e., 340 mbar), we could achieve an energy cost of approximately 0.04 kWh/g compared to 0.19 kWh/g that MOXIE reported to produce O_2 [1,5]. In conjunction with 47 g/h of O_2 production, we also showed that other valuable chemicals, such as key molecules like CO and NO_x, can be produced and utilized in an ISRU context.

In an optical analysis comparing pure CO_2 plasma versus a simulated Mars atmosphere plasma conducted by *Raposo*, it is shown that the conversion process in MW plasma may be enhanced by near-Mars surface pressure conditions (i.e., compared to higher operating pressures) [14]. This thesis outlined the temperature and gas fraction profile of the plasma afterglow when a typical Martian atmosphere surface pressure is used, and it reported a distinct difference in the afterglow chemistry observed by chemiluminescence enhancement, likely attributed to NO + O recombination. Furthermore, *Raposo* states that the presence of Ar plays a significant role in the ionization and dissociation processes. Although more research is needed to confirm these findings, the author infers that the overall rate of CO_2 dissociation is increased in a Martian mixture, likely due to the presence of Ar and N_2. Notably, the author reflects a change in the plasma regime from a homogenous to a contracted plasma (i.e., increasing the intersection of the plasma filament and the transiting gas) with increased pressure from 6 mbar to 300 mbar [14], an observation well reported by *Wolf et al.* in pure CO_2 [16].

In this work, we investigate the benefits of using MW plasma technology for the conversion of a Martian atmosphere-like mixture (with a composition of approximately 96% CO_2, 2% N_2, and 2% Ar) into life-

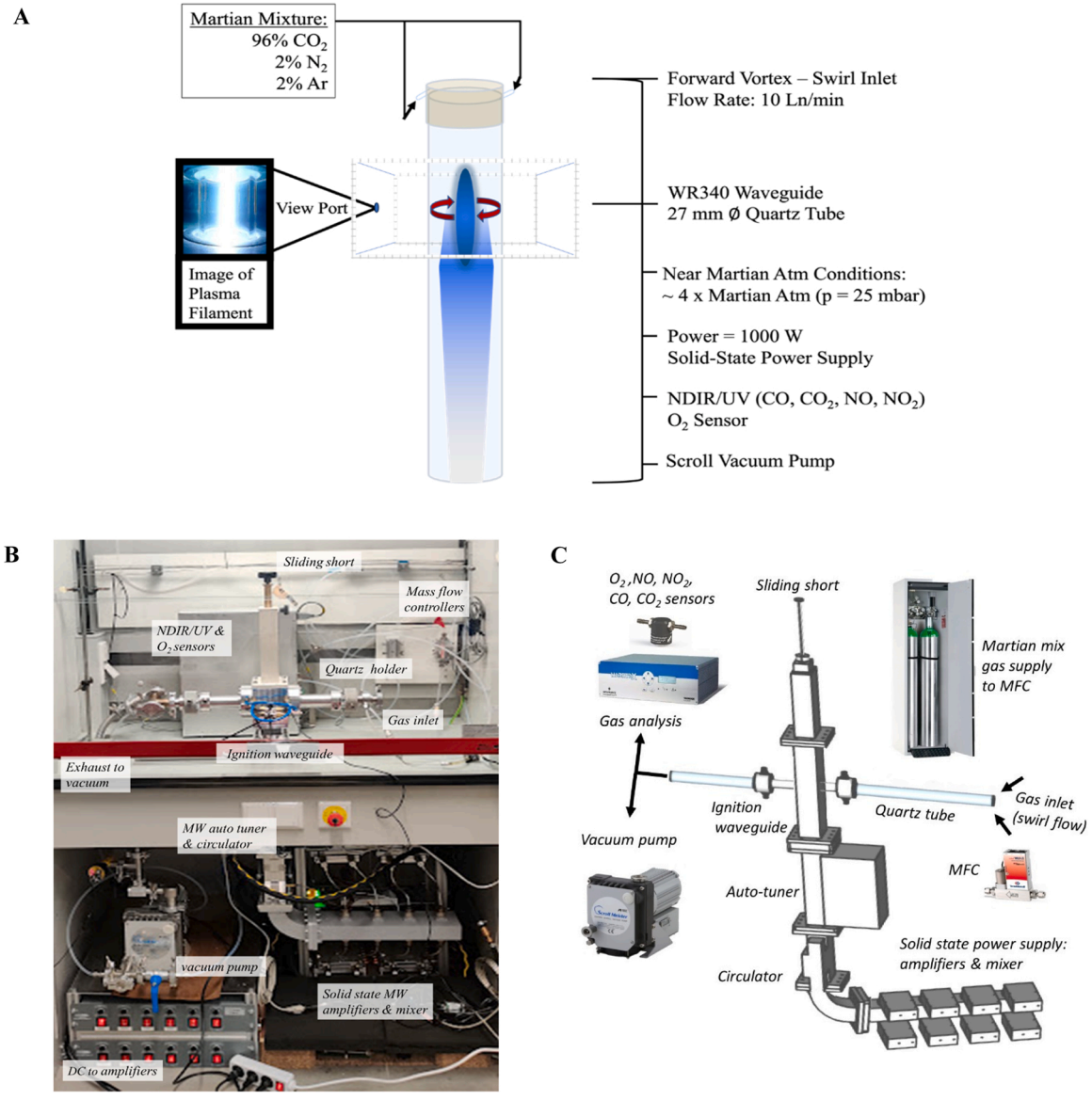

Fig. 1. A. Schematic overview of the 2.45 GHz plasma reactor with a Martian simulant atmosphere at 25 mbar pressure and 1 kW power. The ignition occurs in the coupling chamber of the rectangular WR340 waveguide, where the plasma is stabilized in the center of the quartz tube. The viewing port allows for real-time plasma imaging, as seen in the image of the plasma filament. B. Corresponding photograph of the MW plasma reactor installation in a fume hood at PLASMANT laboratories at the University of Antwerp, with key components labelled. Note the quartz tube is mounted horizontally through the coupling hole in the ignition waveguide with gas flowing from right to left. C. Scheme of the full setup, with key components labelled.

sustaining chemicals at near-Mars surface pressure conditions (25 mbar). We pay special attention to ascertaining the key performance metrics at these low pressures (i.e., key species production rates and energy costs) with support from kinetic modeling to understand the fundamental chemistry. These key aspects, crucial to understanding MW plasma technology for gas conversion on Mars, have not been previously investigated. Notably, the conversion process involves dissociating CO_2 and N_2 molecules, creating target molecules, such as CO, O_2, and NO_x, which can be used as building blocks for liquid bi-propellants and fertilizers. The proposed method can provide valuable resources for future human missions to Mars.

2. Materials and methods

2.1. Experimental setup

The experiments used a forward vortex waveguided configuration with a 2.45 GHz solid-state power supply composed of laterally diffused metal oxide semiconductor (LDMOS) power amplifiers. The output from the amplifiers is combined and guided through an isolator and auto-tuner to the WR340 coupling chamber. A 27 mm inner diameter quartz reaction chamber is perpendicularly mounted through a waveguide terminated by a sliding short, where plasma ignition occurs. The auto-tuner matches the electric field transition into the waveguide/plasma area such that the reflected power is kept below 1% for all conditions. Fig. 1A shows a schematic drawing of the waveguide coupling chamber, where the plasma was ignited in a simulated Martian atmosphere. The gas is injected using a helical swirl inlet to sustain a vortex flow within the discharge area. After that ignition, a surface-wave mode is generated and sustained, isolating the extreme temperatures (~ 6000 K core plasma temperature [9]) from the quartz tube walls. Fig. 1B shows the corresponding photograph of the full experimental setup with key components highlighted while Fig. 1C illustrates the full experimental scheme.

2.2. Measurement techniques and analysis

The post-plasma composition was analyzed using Non-Dispersive Infra-Red and UltraViolet (NDIR/UV) absorption spectrometry (Rosemount X-STREAM XEGP Continuous Gas Analyzer) for NO, NO_2, CO, CO_2 molecules, whereas O_2 was measured using an Infra-Red luminescent quenched absorption technique (Pyroscience GmbH FDO2 Optical Oxygen Sensor) [5,17,18]. In calibrating these diagnostic instruments, we utilize pre-mixed calibration gases (Air Liquide, e.g., NO 16% in Helium and NO_2 7.8% in Helium). Cross-checks using Gas Chromatography (GC) with Interscience Compact GC are also performed. This GC features two channels, each equipped with a Thermal Conductivity Detector (TCD), Carboxen, and Molsieve columns (1010 PLOT and 5 A, respectively). These are used to detect O_2, N_2, and CO, while two RT Q-bond columns (one with a length of 3 m and the other 10 m) are utilized for the detection of CO_2 [9].

The primary gas converted in our experiments is CO_2 (~ 96% of the Martian atmosphere), with oxidation of the small N_2 content (~ 2%). The argon fraction (~ 2%) is not converted due to its inertness. The key overall reactions for consideration are therefore:

$$2CO_2 \rightleftharpoons 2CO + O_2 \quad \text{(Reactionn 1)}$$

$$O_2 + N_2 \rightleftharpoons 2NO \quad \text{(Reactionn 2)}$$

$$2O_2 + N_2 \rightleftharpoons 2NO_2 \quad \text{(Reactionn 3)}$$

During any gas conversion process, the changes in stoichiometric proportions result in changes in the molar flow rate in the plasma exhaust compared to the inlet flow. In our experimental setup, CO_2 is the primary component of the gas fraction. When it is converted into CO and O_2, it leads to an expansion of the inlet flow, which means an increase in the molar flow rate. The extent of this increase is directly related to the degree of conversion. It's worth noting that the formation of NO_2 results in gas contraction; however, due to the relatively small proportion of N_2 and an even smaller fraction of NO_2 formed in comparison to CO and O_2, this contraction effect is negligible when compared to the expansion resulting from CO_2 conversion; therefore, it is neglected in our analysis.

In our case, given the predominant CO_2 conversion, we can infer the degree of expansion by examining the CO_2 conversion as follows [5]:

$$\alpha = 1 + 0.5 * \eta_{CO_2}^{converted} \quad (4)$$

$$\eta_{CO_2}^{converted} = \frac{\eta_{CO_2}^{In} - \alpha * \eta_{CO_2}^{Out}}{\eta_{CO_2}^{In}} \quad (5)$$

Where α represents the gas expansion factor (i.e., $\alpha > 1$), $\eta_{CO_2}^{converted}$ is the fraction of CO_2 converted, $\eta_{CO_2}^{In}$ is the fraction of CO_2 in the mixture when the plasma is off (i.e., 0.96 in our case) and $\eta_{CO_2}^{Out}$ is the measured CO_2 fraction when the plasma is ON (notably we do not add a dilution gas to measure the gas expansion in our experiments [19] with the conversion approximated as a pure CO_2 conversion given the negligible effects of the N_2 conversion in our context [5]). Rearranging Eqs. 4 and 5 we can solve them to find α based on the measured CO_2:

$$\alpha = \frac{1.5 * \eta_{CO_2}^{In}}{\eta_{CO_2}^{In} + 0.5 * \eta_{CO_2}^{Out}} \quad (6)$$

Subsequently, when calculating α, we obtain the CO_2 conversion by Eq. 5. The CO, O_2, and NO_x production rates are calculated based on the fraction of each species measured in the exhaust ($\eta_{CO/O_2/NO_x}$), their molar mass (μ_{CO,O_2,NO_x} [g/mol]), the inlet mass flow rate (f_{in} in normal liters per minute [Ln/min]), as well as α. The individual production rates (PR [g/h]) are then calculated for CO, O_2, and NO_x (NO +NO_2) as:

$$PR_{CO,O_2,NO_x}[g/h] = \frac{\eta_{CO,O_2,NO_x} * \mu_{CO,O_2,NO_x}[g/mol] * \alpha * f_{in}[Ln/\min]}{22.4[L/mol]} * 60[\min/h] \quad (7)$$

22.4 [L/mol] is the molar volume of a gas under the corresponding normal conditions (i.e., T = 273.15 K and p = 1.01325 bar) for which our mass flow controllers (Bronkhorst) are calibrated.

The energy cost (*EC*) to produce CO, O_2, or NO_x is then obtained using:

$$EC_{CO,O_2,NO_x}[kWh/g] = \frac{Power[kW]}{PR_{CO,O_2,NO_x}[g/h]} \quad (8)$$

where the Power [kW or kJ/s] is the absorbed MW power measured during steady-state plasma operation. Additional details regarding the setup can be found in our earlier work [5].

2.3. Numerical modelling

To gain a fundamental understanding of the chemistry in our experiments, we employed a quasi-1D chemical kinetics model using the ZDPlasKin (Zero-Dimensional Plasma Kinetics) solver [5,17,18,20]. The temporal evolution of species densities, encompassing electrons and various charged and neutral species, is determined through balance equations, which consider production and loss terms resulting from chemical reactions. The gas velocity undergoes dynamic changes due to variations in temperature and stoichiometry within the gas mixture, and these changes are updated at each time step. The power density is derived from experimental measurements of absorbed power (i.e., forward minus reflected power) combined with the determination of plasma volume through camera imaging within the waveguide. The assumed shape for the plasma volume is cylindrical [21], consistent with vortex-stabilized discharges. Indeed, in such discharges, the plasma is confined within the inner region of the tube, separated from

containment walls by a swirling or vortex flow boundary, elongating along the flow direction, forming a cylindrical shape [16,21,22].

To address radial variations in power density from the center to the edge of the plasma filament, light emission across the radial extent of the filament at its ignition point inside the waveguide is used as a proxy for the plasma width. The quasi-1D model is applied to two radial sections, representing high power density at the plasma core and relatively low power density to simulate the plasma edge, as explained in our earlier publication [17]. For each quasi-1D model, a triangular distribution of power density is assumed in the lateral extent of the plasma, aligned with earlier models of power dissipation in surface wave-sustained MW plasmas [23,24]. To simulate electron dynamics, we employ the Boltzmann solver BOLSIG+ , linking plasma conductivity (a function of the reduced electric field) to electron mobility. The gas temperature is computed at each time step in the model by the gas thermal balance equation under isobaric conditions, accounting for gas heating from elastic collisions between electrons and gas molecules, enthalpy contributions from chemical reactions among plasma species, heat losses to walls, and dynamic heat capacity considering the gas mixture. More detailed information can be found in our earlier works [5,17,20,25].

The reaction scheme for the Martian atmosphere (96/2/2% v/v CO_2/N_2/Ar) used in this study is compiled from our prior research efforts, with complete details given in our earlier publications [5,25–27]. The model encompasses 148 distinct species, including electrons, CO_2, Ar, N_2, O_2, CO, various N_xO_y molecules in ground state, as well as different (vibrational and electronic) excited levels, radicals, atoms, and ions (see Table 1), which undergo interactions through 973 electron impact reactions and 12,604 heavy particle reactions, involving molecules in ground state or excited levels, radicals, atoms, or ions. The rate coefficients for the heavy species reactions are drawn from our previous works, whereas the rate coefficients for electron impact reactions are computed using the Boltzmann solver BOLSIG+ [28] integrated into ZDPlasKin.

Due to the relatively inert nature of N_2 and CO_2, considerable energy is required for thermal conversion; however, plasma-based conversion provides additional reaction pathways. This is especially the case in low pressure MW plasma [16] where the electrons have the energy needed to induce excitation towards the lowest vibrational levels in CO_2/N_2 (~1 eV), followed by further vibrational-vibrational (V-V) collisions, which enable a "ladder-climbing" process, gradually populating higher vibrational levels (denoted as $CO_2(v)$ and $N_2(v)$). In addition, there can be significant populations of electronically excited molecules (i.e., CO_2(E) and N_2(E)), which form inside the plasma region. In contrast to a purely thermal case, these molecules serve to lower the overall energy required for CO_2 and N_2 dissociation (i.e., O_2 formation and NO_x formation), as their higher energy levels will help to overcome the activation barriers.

Table 1
Species simulated in the quasi-1D kinetic model for a CO_2/N_2/Ar Martian mixture.

Neutral	Excited	Charged
CO_2, CO, C_2O, C, C_2, CN, ONCN, NCO, NCN, C_2N, C_2N_2	$CO_2(V_a, V_b, V_c, V_d)$, $CO_2(V_1$-$V_{21})$, $CO_2(E_1)$, $CO(V_1$-$V_{10})$, CO (E_1-E_4)	CO_2^+, CO_4^+, CO^+, $C_2O_2^+$, $C_2O_3^+$, $C_2O_4^+$, C_2^+, C^+, CO_3^-, CO_4^-
O_2, O, O_3	$O_2(V_1$–$V_{15})$, $O_2(A_1\Delta)$, $O_2(A_3C_3C_1)$[a], $O_2(B_1\Sigma)$, O(1D), O (1 S)	e, O^+, O^-, O_2^-, O_2^+, O_4^-, O_4^+, O_3
N_2, N, NO_2, NO, N_2O, N_2O_3, N_2O_4, N_2O_5	$N_2(V_1$–$V_{21})$, $N_2(A_1\Sigma)$, $N_2(A_3\Sigma)$, $N_2(B_3\Pi)$, $N_2(C_3\Pi)$, N(^{2}D), N(^{3}P)	N_2^+, N_3^+, N_4^+, N^+, NO_2^+, NO_2^-, N_2O^-, N_2O^+, NO^+, NO^-, NO_3^-
Ar	Ar(^{4}S), Ar(^{4}P), Ar_2(E)[b], Ar ($^4S^3[P_0]$), Ar($^4S^3[P_1]$), Ar ($^4S^3[P_2]$), Ar($^4S^1[P_1]$)	Ar^+, Ar_2^+

[a] : $O_2(A_3C_3C_1)$ is a combination of three electronically excited states $O_2(A^3\Sigma)$, $O_2(C^3\Delta)$ and $O_2(c^1\ \Sigma)$ with a threshold energy of 4.5 eV.

[b] : Ar_2(E) is a combination of the excited states $Ar_2(^1\Sigma)$ and $Ar_2(^3\Sigma)$ of the Ar_2 dimer.

NO_x production (overall Reactions 2 and 3 above) in plasma depends on atomic nitrogen (N) and oxygen (O) formation. In a plasma, this can also proceed via an electronically or vibrationally enhanced Zeldovich mechanism [29–31] consisting of the following reactions:

$$O + N_2/N_2(E,v) \rightleftharpoons N + NO \quad \text{(Reactionn 9)}$$

$$N + O_2/O_2(E,v) \rightleftharpoons O + NO \quad \text{(Reactionn 10)}$$

Given the strong N_2 triple bond, the above reaction pair is typically rate-limited by Reaction 9**.** Compared to the purely thermal Zeldovich mechanism (i.e., involving only ground state N_2 and O_2), plasma-based conversion has the additional presence of vibrationally or electronically excited N_2 and O_2 molecules, which lower the dissociation threshold required to break the N_2 bond (~9.8 eV) by colliding with O atoms (Reaction 9). The N atoms formed here further react with both ground state and vibrationally/electronically excited O_2 molecules (Reaction 10) to produce another NO. Reaction 10 also produces an additional O atom, which can again react with ground state and vibrationally/electronically excited N_2 molecules (Reaction 9). Furthermore, it can oxidize NO to produce NO_2:

$$NO + O \rightleftharpoons NO_2 \quad \text{(Reactionn 11)}$$

When considering CO_2 dissociation, a similar reaction pathway applies. The overall reaction shown in Reaction 1 above includes the following elementary sub-reactions involving atomic oxygen:

$$CO_2(E,v) \rightleftharpoons CO + O \quad \text{(Reactionn 12)}$$

$$CO_2(E,v) + O \rightleftharpoons CO + O_2 \quad \text{(Reactionn 13)}$$

Direct dissociation processes in Reaction 12, such as electron impact dissociation, have an energy threshold of 5.5 eV to overcome the (ground state) CO_2 bond energy, but the O atom produced in Reaction 12 can further react (i.e., Reaction 13) with CO_2 (and its vibrationally or electronically excited states). This coupling lowers the threshold considerably (e.g., for ground state CO_2, this lowers the overall energy threshold to 2.9 eV [8]).

3. Results and discussion

3.1. Experimental results

We discuss our experimental results using our solid-state surface-wave MW plasma reactor, modified for operation at reduced pressures close to Martian ambient conditions. All experiments were carried out using the 2.45 GHz MW reactor described in the ***Materials and Methods*** section, with a flow rate = 10 Ln/min (i.e., 1131 g/h CO_2, 30 g/h N_2, and 21.4 g/h Ar mass flow rate for a Martian mixture in a ratio 96/2/2 v/v CO_2/N_2/Ar), a pressure of 25 mbar, and 1000 W of absorbed plasma power. Throughout the text, NO_x indicates the sum of NO and NO_2.

The production rates of CO, O_2, and NO_x (PR_{CO,O_2,NO_x}) measured in the plasma exhaust are presented in Fig. 2(A). For comparison, we have included our previous results, which were investigated under the same pressure conditions as the MOXIE experiments (340 mbar) [5]. The PR_{O_2} was 75.7 ± 0.9 g/h, which is approximately a 50% relative increase over the 340 mbar conditions previously reported. Additionally, the PR_{CO} was 127.7 ± 1.0 g/h, an approximately 66% increase over our previously reported results, and the total PR_{NO_x} was 2.9 ± 0.1 g/h, i.e., a factor two higher than our previous results, with an equivalent concentration in the exhaust mixture of 3015 ± 14 ppm (or ~ 0.3%). The primary species produced were NO and NO_2, with a ratio of NO/NO_2 of approximately 9 (i.e., NO concentrations dominate), corresponding to approximately 15% of the N_2 inflow being fixed. We can thus conclude that reducing the pressure closer to Mars' ambient conditions increases the overall production of CO/O_2/NO_x, despite a significant reduction in

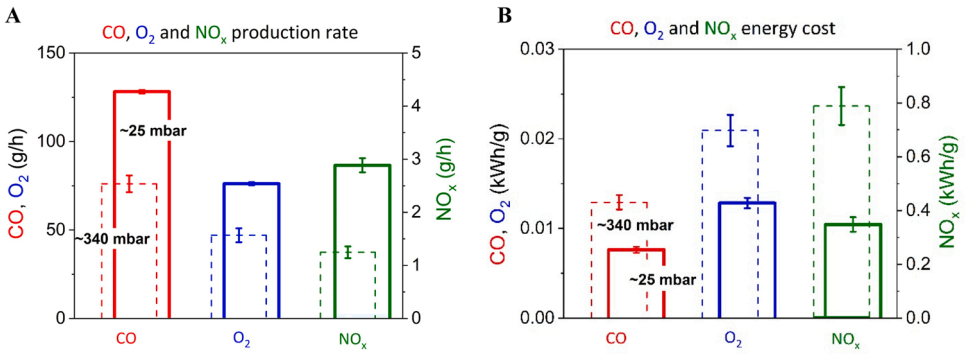

Fig. 2. Comparison of (A) production rate, and (B) energy cost, at a pressure of 25 mbar (or ~3.5 Martian atm) with 340 mbar (dashed lines) [5]. Martian mix at 10 Ln/min, 1 kW. Note the NO_x data is indicated in the right-hand y-axes in both graphs.

gas residence time under the low-pressure conditions by nearly a factor of ten. Overall, the sampled exhaust mixture has a percentage ratio of approximately 15.9% CO, 8.3% O_2, and 0.3% NO_x.

Furthermore, in Fig. 2(B) we observe that the corresponding EC_{CO} is 0.0080 ± 0.0004 kWh/g, the EC_{O_2} is 0.013 ± 0.006 kWh/g, and the EC_{NO_x} is 0.35 ± 0.03 kWh/g. Given the boost in PR_{CO,O_2,NO_x}, the *EC* drops similarly by approximately 50 – 70% for O_2 and CO, respectively, and by more than a factor two for NO_x under these reduced pressure conditions, when compared to our previous work [5].

It is evident by these results that plasma-based conversion of CO_2 and fixation of N_2 is significantly more productive at pressures resembling the Martian environment. This is likely due to vibrational excitation, as these levels are known to be overpopulated in plasmas at lower pressure because of the reduced losses upon collisions with ground state molecules. This results in a more pronounced vibrational-translational non-equilibrium, which gives rise to the most efficient conversion routes [6, 32]. We explore this further by numerical modeling in the next section.

3.2. *Fundamental insights using numerical modelling*

We applied a chemical kinetics model [5,17,20] at near-ambient Martian pressure corresponding to our experimental conditions (i.e., 25 mbar which is ~3.5 times the typical Martian ambient pressure of ~7 mbar) in order to gain a deeper fundamental understanding of the mechanisms behind the observed gains in production rate (PR_{CO,O_2,NO_x}) and the lower energy cost (EC_{CO,O_2,NO_x}). In Fig. 3, we plot the calculated concentrations of CO, O_2 and NO_x as a function of position, in the *active plasma region* (between 0 and 20 cm) and in the afterglow region (between 20 and 35 cm), where a steady state is eventually reached. The experimentally measured concentrations in the effluent, as reported above, are indicated with stars for comparison.

As shown in Fig. 3(A), an O_2 concentration of 8.2% is predicted at 35 cm, downstream of the plasma region, which is within the error value of the measured concentration of 8.3 ± 1.1%, as indicated by the star. The CO concentration predicted by our model is approximately twice the O_2 concentration, with a value of 17.6% at the same position downstream. This value compares reasonably to our experimental measurement of 15.9 ± 0.7%.

Fig. 3(B) demonstrates that at 35 cm downstream, our model predicts a steady-state total concentration of NO_x to be approximately 6777 ppm. Compared to the total measured NO_x concentration (ca. 3000 ppm), our model overestimates NO_x production by more than a factor of two. This overestimation is attributed to the relatively small number of N_2 levels simulated, the complexity of the underlying chemistry relying upon thousands of empirical reaction rate coefficients, and the inherent physical approximations required in quasi-1D models. Given the deviation found in the predicted NO_x concentration in our earlier work at 340 mbar (factor ~ four), the deviation here (factor ~ two) is reasonable to expect. However, we believe that the model can still provide valuable insight into the dominant production mechanisms.

Fig. 4 presents an overview of the modeling results in terms of CO_2 dissociation pathways. Taking an average across the simulation domain, we find that CO and O_2 are primarily formed via Reaction 13, involving the collision of O atoms with CO_2, yielding CO and O_2. Our analysis reveals that 79% of the CO and O_2 produced via Reaction 13 involves the symmetric stretch and bending vibrational modes of CO_2, namely $CO_2(v_a\text{-}v_d)$ (ranging 0.08 – 0.33 eV in energy) [33], while 7% occurs from ground state CO_2. In contrast to the pressure conditions at 340

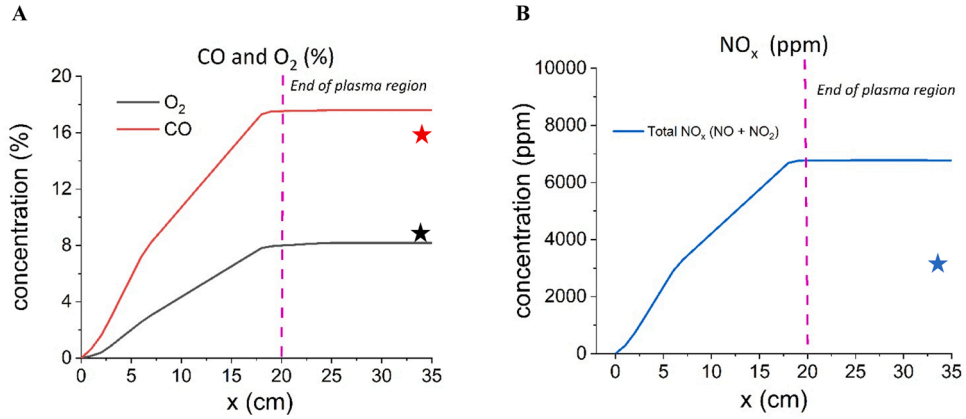

Fig. 3. Calculated CO, O_2 (A) and NO_x (B) product concentrations as a function of position in and after the MW plasma, using a Martian simulant mixture (96/2/2% v/v $CO_2/N_2/Ar$) at a flow rate of 10 Ln/min, a pressure of 25 mbar, and 1 kW of absorbed power. The measured CO, O_2 and NO_x concentrations downstream (hence, after the plasma) are indicated with stars, for comparison.

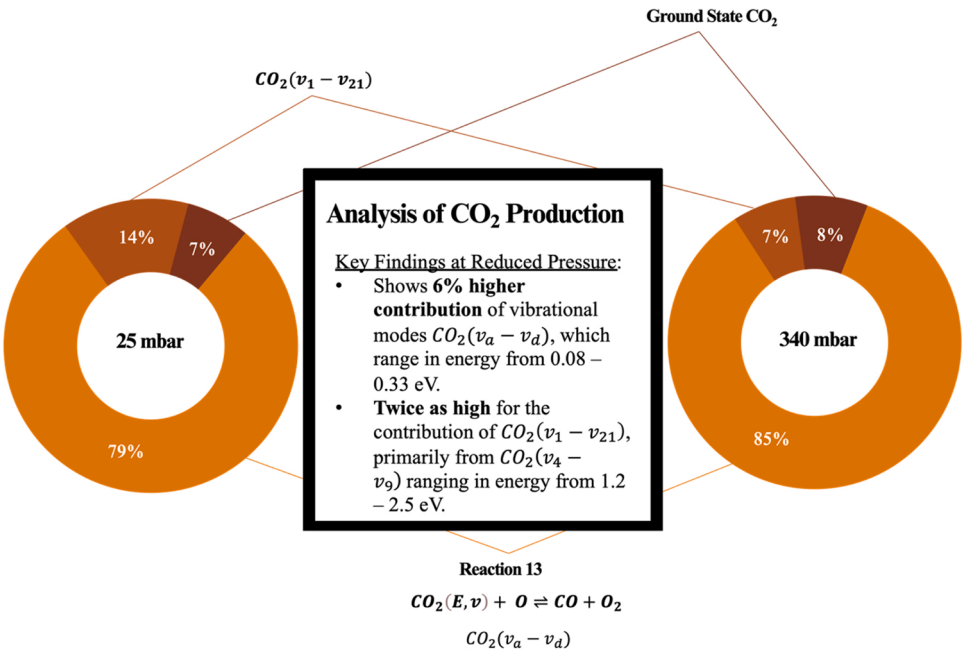

Fig. 4. Analysis of CO_2 dissociation mechanisms from the ZDPlaskin model with a highlight of the key findings. We directly compare these model results with the results of our previous work [5].

mbar in our earlier work, we observe approximately double the contribution from the asymmetric stretch vibration mode, $CO_2(v_{1-21})$, with 14% at 25 mbar, which we find to originate primarily from additional contributions from $CO_2(v_{4-9})$ (ranging 1.2 – 2.5 eV in energy). The contribution of the symmetric stretch and bending modes remains high, with a slight drop from 85% at 340 mbar to 79% at 25 mbar. Finally, the contribution from the ground state remains similar (i.e., 8% vs. 7%) despite the almost tenfold drop in pressure.

Fig. 5 provides an overview of the NO production mechanisms predicted by the ZDPlasKin model. The contribution of the first Zeldovich reaction (Reaction 9) between N_2 and O atoms increases to 67% at 25 mbar, compared to our previous results, where this reaction contributed 51% at 340 mbar. Notably, $O_2(v_{1-2})$ has a larger contribution here at 25 mbar, increasing to 8% from 5% at 340 mbar. Furthermore, ground state contributions increased to 16% at 25 mbar from 13% at 340 mbar. The role of the other $O_2(v)$ levels and the $O_2(E)$ had a negligible contribution under both pressure conditions.

This Zeldovich reaction is facilitated by electronically or vibrationally excited N_2 molecules. Indeed, the N_2 molecules in the ground state play a negligible role in NO formation, both at 25 and 340 mbar. The $N_2(E)$ molecules contribute 14% at 25 mbar, significantly lower than the 43% we observed at 340 mbar. On the other hand, the vibrationally excited $N_2(v)$, mainly from levels near the threshold energy for N_2 oxidation ($v = 10 - 14$), contributed for 53% to the overall NO formation at 25 mbar, compared to only 9% at 340 mbar. As the production of $N_2(v)$ requires less energy than of $N_2(E)$, i.e., the excitation energy for $N_2(v)$ ($v = 10 - 14$) is in the range 2.7 - 3.7 eV, while for $N_2(E)$ it is over 6.2 eV, this explains why the energy cost for NO production at 25 mbar

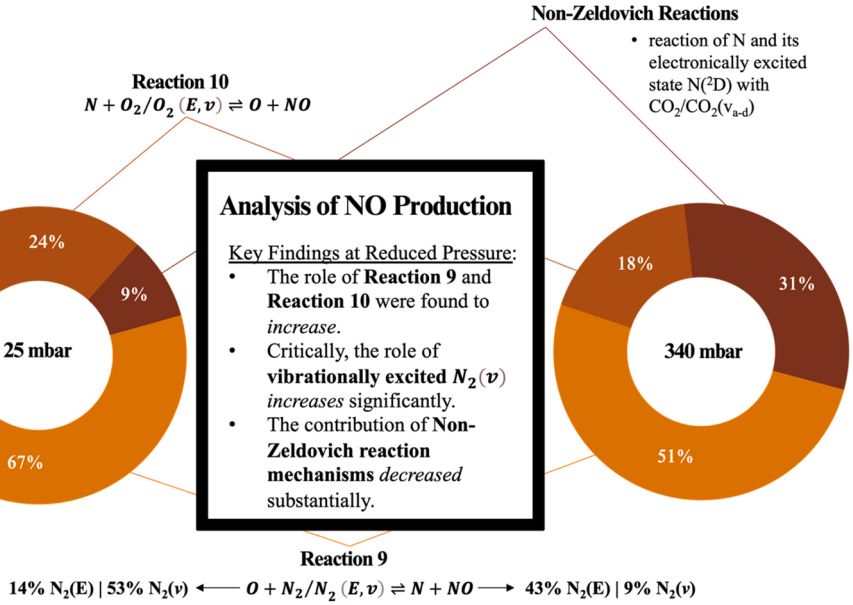

Fig. 5. Overview of NO production mechanisms from ZDPlasKin model.

is more than a factor two lower than at 340 mbar (see Fig. 2). When we analyze the role of the second Zeldovich reaction (Reaction 10), we find that it contributes 24% to the overall NO formation at 25 mbar, increasing to 8% from 5% at 340 mbar. Notably, $O_2(v_{1-2})$ has a larger contribution at 25 mbar, increasing to 8% from 5% at 340 mbar, while the ground state contribution increases to 16% at 25 mbar, from 13% at 340 mbar. The other $O_2(v)$ levels and O_2(E) have a negligible contribution under both pressure conditions.

The remaining NO is created from non-Zeldovich reactions, contributing 9% at 25 mbar, mainly due to the reaction of N and its electronically excited state, N(^{2}D), with $CO_2/CO_2(v_{a\text{-}d})$, making up approximately 7% of the overall reaction. The weight of this reaction is increased at higher pressures, where we observed a stake of 30% at 340 mbar [5] following the exact mechanisms, with the reaction of N/N(^{2}D) with $CO_2/CO_2(v_{a\text{-}d})$ contributing approximately 19%. As this reaction is less energy-efficient than the vibrationally and electronically enhanced Zeldovich mechanism, we can conclude that this heavily affects the overall energy cost of NO formation and is the reason why our results show a drop in energy cost by more than a factor of two compared to the results at 340 mbar (cf. Fig. 2).

In summary, our model predicts that most NO formation at 25 mbar occurs by a combination of the electronically and vibrationally enhanced Zeldovich reactions (Reaction 9 and Reaction 10), with a total contribution of 91%. Most strikingly, the contribution of vibrationally excited $N_2(v)$ increases significantly at lower pressures, explaining the boost in production and drop in energy cost of NO formation at 25 mbar vs 340 mbar.

An important factor in utilizing the near-ambient Martian pressure (25 mbar), while keeping the same mass flow rate as in our earlier work, is the limited residence time of the gas in the plasma region at reduced pressures. At 340 mbar, the gas is found to spend approximately 75 ms within the plasma region (i.e., 0 – 20 cm). At 25 mbar, using the same mass flow rate of 10 Ln/min, the gas spends approximately 7.5 ms within the plasma region. Therefore, exploiting the benefits of low-pressure conditions while elongating the gas residence time within the plasma, by applying a lower mass flow rate or creating a longer plasma, could have further benefits to conversion. This will be explored in our future work.

3.3. Plasma-based IRSU on Mars

As we have outlined, plasma-based conversion of Martian atmosphere enables not only O_2 production but also the formation of CO and NO_x. These life-sustaining molecules can be utilized as IRSU precursors for both fuels and fertilizers. Numerous studies have shown that ISRU on Mars will be essential in realizing cost-effective missions and future colonization of The Red Planet [15,34–36]. To explore Mars, we need propulsion systems that require less mass to be launched from Earth, as reaching Mars requires substantial resources, although the exact amount of propellant will depend on the weight of the launch vehicle and mission outline, according to NASA [35].

Plentiful sources of hydrogen have yet to be identified on the surface of Mars; therefore, traditional rocket propellants are likely unavailable for in-situ production. In an article assessing and comparing potential hydrogen-free propellants for an In-situ Mars Ascent Vehicle (IMAV), *Conley et al.* [37] determined that a liquid propulsion system using a mixture of CO and O_2 was the most favorable regarding performance, safety, and feasibility. The CO/O_2 propellant combination is a top candidate for a Martian in-situ propellant rocket engine, and the feasibility of a pump-fed engine has been detailed in a report by *Roncace et al.* [38]. As we have shown, plasma conversion of Martian atmosphere can provide a low energy cost method to produce this bipropellant.

In May 2008, the Phoenix Scout Mission landed on the surface of Mars in search of water and signs of life. Within the data, the Martian regolith was found to consist of essential nutrients for plant growth, including both macronutrients, such as oxygen, carbon, hydrogen, nitrogen, potassium, phosphorus, calcium, magnesium, and sulfur, and micronutrients, such as iron, manganese, zinc, copper, molybdenum, boron, and chlorine [39–41]. The Martian regolith was also shown to be laced with an abundance of heavy metals and, of particular interest, perchlorates, which can be highly toxic to humans if ingested or inhaled. This will pose a significant issue for future explorers, as any heavy metals will be taken up by the plants and subsequently consumed by Martian colonists. Furthermore, perchlorates pose a chemical hazard to any astronauts on Mars [42–44]. Nevertheless, many studies have been conducted on the feasibility of growing plants on the surface of Mars with fair success using Martian soil simulants [40,41]; however, it is clear that due to the nature of Martian regolith, inoculation of organic matter and fertilizer to the growth medium will be critical to crop success, which will be a critical resource for self-sufficient colonies. Although the production of NO_x species from plasma-based application will most likely not be the only source for enrichment of Martian regolith, it is a key product formed in the dissociation of Mars atmosphere that can be utilized in the production of ISRU fertilizers.

3.4. Post-plasma separation: harnessing the martian atmosphere

As outlined in the previous section, plasma-based conversion of Martian atmosphere provides a gateway to produce O_2, CO, and NO_x as precursors to bi-propellants and fertilizers. The challenge lies in efficiently separating these value-added molecules in the post-plasma effluent mixture. Various separating schemes exist in industry [45–51], including several hybrid designs, combining gas separation by pressure swing adsorption (PSA), vacuum swing adsorption (VSA), or temperature swing adsorption (TSA); however, in theory, the most promising separation scheme for this application is vacuum and temperature swing adsorption (VTSA), to profit from the available low pressure at the Martian surface and the heat generated by the MW reactor.

Furthermore, Oxygen transport membranes (OTMs) for O_2 separation can be utilized in the separation from the post-process stream [52]. These are comprised of a material that is conductive for oxygen ions and electronic charge carriers (electrons, defect electrons). The OTMs are referred to as mixed ionic electronic conductor (MIEC) membranes or ion transport membranes (ITMs), with the driving force for O_2 permeation created by the difference of partial pressures of oxygen (pO_2) determined by a gradient of oxygen vacancies across the membrane [53]. The oxygen ion transport mechanism is a thermally activated process; therefore, such membranes work at high temperatures, typically 800 °C – 1300 °C. The post-plasma region of a MW plasma falls well within this temperature range [9]. Among the studied OTM materials, $Ba_{0.5}Sr_{0.5}Co_{0.8}Fe_{0.2}O_{3-\delta}$ (BSCF) appears to be among the most promising for O_2 separation from a gas mixture, showing excellent performance in terms of oxygen flux and separation [52,54,55]. Although promising, it should be noted that BSCF has shown inadequate chemical stability when in contact with reacting gases such as CO_2, CO, and NO_x [56,57], which poses a significant challenge. It is theoretically possible to address this by operating the membranes in a “protected” mode. A scheme for this might consider utilizing a VTSA unit for purifying the effluent mixture before these reacting gases come into contact with the OTM. Following this, the permeated oxygen could be removed by vacuum on the permeate side of the membrane, followed by pressurizing or condensing using cryopumping equipment.

Finally, it is feasible to utilize VTSA units to separate and recycle unreacted CO_2, N_2 and Ar back into the reaction stream. This could be achieved by using a multi-layer structure of adsorbers following the conversion characteristics of the plasma reactor, as well as the needs of post-plasma processing, such as protecting the OTM. The separately collected gases could then be pressurized or condensed using cryopumping for storage and later use. In a continuous plasma process, converted gas can be stored in intermediary equipment and, following industrial standards, should be made of at least two capacities installed

in parallel that are cyclically compressed and connected to the VTSA unit. In some of the proposed gas separation schemes, particularly relating the introduction of inert gas, such as Ar (recovered and recycled in the separation system), has been considered to enhance the separation performance.

3.5. Technological readiness and future prospects

Currently, plasma-based gas conversion has a Technology Readiness Level (TRL) of approximately 3, i.e., achieved experimental proof of concept [58]. Growing commercial interest in nitrogen fixation, carbon utilization, and hydrocarbon (e.g., methane) reforming are expected to drive the general readiness of the technology in the years to come [8,59] Plasma technology in an ISRU context is less developed than Earth-based applications, with an estimated TRL of 1 – 2, i.e., basic principles and technology concepts formulated. Progress for Earth-based applications, however, should significantly speed up the development of plasma technology for ISRU and aerospace, with substantial overlap and complementarity anticipated.

Most importantly, considerable evidence suggests that the technological and scientific advances that stem from space exploration hold tremendous potential for propelling humanity forward. These state-of-the-art advancements can contribute to addressing global issues, such as climate change. They also have the additional advantage of more intangible benefits, such as inspiring more individuals to pursue careers within science and technology, furthering the collective 'minds' seeking the expansion of human knowledge [60–62]. Many have proposed plasma-based technology as a Power-2-X technology that can help combat climate change by introducing a circular economy for carbon emissions [59,63–65]. By employing this technology in an ISRU context for Mars, it is possible that we can realize the potential for ISRU here on Earth as well.

The new generation of solid-state Radio Frequency (RF) is driven by cellular communications, where there's a need for high power linearity that is created by transistors and semiconductors. The approach generates a stable, efficient, and, more importantly, controllably reproducible signal that magnetron-based reactors could never realize [66,67]. As a result, solid-state MW power systems have some enticing advantages, which are particularly interesting for aerospace and ISRU applications. They are a considerably more compact and portable form factor compared to bulky and high-voltage-powered magnetron systems [66]. The technology is also frequency- and phase-stable in coherent systems, which allows the power combining of generators to deliver an extensive power range or distributed power sources into large geometries [66]. Modularity is impossible with magnetron technology or would entail bulky waveguide distribution systems. Furthermore, solid-state technology offers much improved operational longevity over magnetrons (i.e., $>$ 100,000 vs. 8000 h lifetime) and better mechanical ruggedness. The magnetron filaments are sensitive to mechanical shock (like those created during rocket starts). Notably, the magnetron is a "single point of failure" power source, while solid-state generators typically consist of several sub-units; therefore, if a failure occurs in one or more sub-units, the system can still function [66]. Also, the efficiency of contemporary solid-state MW power supplies is comparable with mature magnetron technology in many instances, with efficiency levels of $>$ 60% possible, even for 2.45 GHz systems [61,68]. Hence, solid-state systems will not deteriorate in power output or efficiency like magnetron sources. The solid-state RF generators detailed above are ideal for ISRU, aerospace, aeronautics, and defense applications. This mature technology underpins today's cellular network capabilities on Earth. Moreover, it surpasses tube-based amplifiers in weight, size, and modularity.

Radiation hardness is a concern on Mars due to the lack of a protective ionosphere, exposing it to a high-energy radiation [35,60]. Although radiation affects semiconductors, smaller devices, and active components exhibit reduced sensitivity. The gallium nitride (GaN) semiconductor, with its high energy density and small device area per transistor, is remarkably robust against radiation and is already prevalent in advanced aerospace and defense sectors [60,61]. Furthermore, GaN offers benefits in miniaturization and weight reduction over traditional RF semiconductors like LDMOS. In essence, the semiconductor-based RF generators discussed in this paper hold great potential for Mars ISRU missions.

4. Conclusion and outlook

Mars presents favorable low-pressure conditions ideal for efficient conversion through vibrationally-induced dissociation pathways of CO_2 and N_2 using solid-state MW plasma reactors, positioning such devices as promising candidates for In-Situ Resource Utilization (ISRU). However, the potential of these devices in the context of ISRU remains largely untapped [5,13–15]. In the MOXIE experiment [2,69], the energy cost to compress from the Martian surface pressure using a scroll pump was about one-third of the total energy cost of the CO_2 conversion into O_2. Hence, the overall energy cost may be considerably reduced if Mars ambient pressure can be used. Our prior research delved into MW plasma-based conversion of Martian atmosphere at the pressure conditions used in the MOXIE experiment, specifically 340 mbar [5], allowing for a more direct comparison of these two technologies and demonstrating the energy-efficient performance of plasma-based ISRU, although it should be realized that the cost of separating the product mix was not yet accounted for. In this paper, we present our experimental findings, bolstered by modeling, from our solid-state surface-wave MW plasma reactor, adapted to operate at pressures closely mirroring Martian ambient conditions, thus avoiding the above-mentioned gas compression costs. We thus compare the conversion near-ambient Martian pressure conditions (25 mbar) to our previous work (340 mbar) [5].

We achieved an O_2 production rate of 75.7 $\pm$ 0.9 g/h, CO at 127.7 $\pm$ 1.0 g/h, and NO_x at 2.9 $\pm$ 0.1 g/h. Remarkably, the rate of O_2 production is about 47 times greater than that of the MOXIE test experiment (~1.6 g/h) [1,2], and this was accomplished at an energy cost of 0.013 kWh/g, i.e., nearly 15 times lower than that of the MOXIE test (0.19 kWh/g). When contrasted with our earlier experiments at higher pressures [5], the tests conducted at 25 mbar showed an increase of 50 – 70% in O_2 and CO production rates. Moreover, roughly 15% of the incoming N_2 transformed into NO_x, exceeding a twofold gain compared to the higher-pressure conditions [5]. This uptick in production, accompanied by a comparable drop in energy cost, was observed despite the gas residence time in the plasma region being reduced by a factor of ten. Our results show that CO_2 conversion and N_2 fixation via plasma are notably more efficient at Martian ambient pressures.

We also performed numerical modeling to reveal the underlying chemical pathways, supporting our experimental findings. We observe an approximate doubling in the contribution from the asymmetric vibrational modes, $CO_2(v_{1-21})$, to CO and O_2 production, from 7% at 340 mbar to 14% at 25 mbar. This explains the higher CO and O_2 production rates and lower energy costs at near-ambient Martian surface pressure. Moreover, our model predicts that NO formation occurs primarily by a combination of the electronically and vibrationally enhanced Zeldovich reactions, a well-known reaction pathway for nitrogen oxidation, with a total contribution increase from 70% at 340 mbar to 92% at 25 mbar. The most significant factor is the contribution of vibrationally excited $N_2(v)$, which appears to be the most efficient pathway for nitrogen fixation compared to the electronic or ground-state species contributions. As this pathway increases at lower pressures, it explains the observed boost in NO production rate and drop in energy cost.

Our MW plasma-based conversion of Martian atmosphere yields a combination of O_2, CO, and NO_x; therefore, separation is essential to fully harness these products in an extraterrestrial ISRU context. Although post-plasma separation is out of the scope of this research, we highlight potential gas separation systems and their theoretical integration with a solid-state MW plasma reactor. However, this integration

is intricate due to numerous parameters and should be carefully considered. Future studies should focus on utilizing a multi-objective optimization strategy, drawing from comprehensive numerical simulations of the entire process. Currently, various components of the gas separation system — including the MIEC membrane module, the dedicated VTSA, cryopumping systems, and the dual-capacity gas pressurizing system — are under construction and simulation at *Air Liquide*. These efforts aim to validate the models intended for scaling the design to meet ISRU-specific applications.

It is clear that exploration and colonization of Mars present enormous challenges that extend beyond just reaching the planet. Establishing a sustainable and self-reliant habitat on a foreign planet requires innovative technologies and efficient resource utilization strategies. Plasma-based applications, as highlighted, offer a promising avenue for advanced chemical conversion in the challenging Martian environment. The capability to produce life-sustaining chemicals and propellants from Mars' atmosphere points to a future where humanity can truly *live off Martian land*. Research geared toward the advancement of space exploration also provides valuable insight into sustainable practices that could benefit civilization as a whole. The lessons learned from these endeavors of achieving ISRU on a foreign planet will undoubtedly shape our approach to sustainability and resource management on our home planet.

CRediT authorship contribution statement

Bogaerts Annemie: Conceptualization, Investigation, Project administration, Resources, Supervision, Writing – original draft, Writing – review & editing. **Cowley Aidan:** Conceptualization, Investigation, Project administration, Resources, Writing – original draft, Writing – review & editing. **Fedirchyk Igor:** Investigation, Writing – review & editing. **Gorbanev Yury:** Investigation, Writing – review & editing. **Mercer Elizabeth:** Investigation, Methodology, Writing – original draft, Writing – review & editing. **Kelly Sean:** Conceptualization, Data curation, Formal analysis, Funding acquisition, Investigation, Methodology, Project administration, Resources, Software, Supervision, Validation, Visualization, Writing – original draft, Writing – review & editing. **Werner Klaus:** Investigation, Resources, Visualization, Writing – original draft, Writing – review & editing. **Verheyen Claudia:** Investigation, Writing – review & editing. **Pullumbi Pluton:** Investigation, Resources, Writing – original draft, Writing – review & editing.

Declaration of Competing Interest

The authors declare that they have no known competing financial interests or personal relationships that could have appeared to influence the work reported in this paper.

Data availability

Data will be made available on request.

Acknowledgements

We acknowledge financial support by a European Space Agency (ESA) Open Science Innovation Platform study (contract no. 4000137001/21/NL/GLC/ov), the European Marie Skłodowska-Curie Individual Fellowship "PENFIX'' within Horizon 2020 (grant no. 838181), the European Research Council (ERC) under the European Union's Horizon 2020 Research and Innovation Program (grant no. 810182; SCOPE ERC Synergy project), the Excellence of Science FWO-FNRS PLASyntH2 project (FWO grant no. G0I1822N and EOS no. 4000751) and the Methusalem project of the University of Antwerp.

References

[1] J.A. Hoffman, et al., Mars Oxygen ISRU Experiment (MOXIE)—Preparing for human Mars exploration, Sci. Adv. vol. 8 (35) (2023) eabp8636, https://doi.org/10.1126/sciadv.abp8636.
[2] A. Cool, Andrew; Fox, Karen; Johnson, "NASA's Oxygen-Generating Experiment MOXIE Completes Mars Mission." Accessed: Oct. 10, 2023. [Online]. Available: ⟨https://mars.nasa.gov/news/9474/nasas-oxygen-generating-experiment-moxie-completes-mars-mission/⟩.
[3] A. Fox, Karen; Johnson, Alana; Skelly, Clare; Good, "NASA's Perseverance Mars Rover Extracts First Oxygen from Red Planet."
[4] K.W. Engeling, R.P. Gott, Plasma for crewed transit and planetary habitation: research efforts at Kennedy Space Center, IEEE Trans. Plasma Sci. vol. 51 (6) (2023) 1568–1579, https://doi.org/10.1109/TPS.2023.3277216.
[5] S. Kelly, C. Verheyen, A. Cowley, A. Bogaerts, Producing oxygen and fertilizer with the Martian atmosphere by using microwave plasma, Chem vol. 8 (10) (2022) 2797–2816, https://doi.org/10.1016/j.chempr.2022.07.015.
[6] R. Snoeckx, A. Bogaerts, Plasma technology – a novel solution for CO_2 conversion? Chem. Soc. Rev. vol. 46 (19) (2017) 5805–5863, https://doi.org/10.1039/C6CS00066E.
[7] V.A. Legasov, et al., A nonequilibrium plasma-chemical process of CO_2 dissociation in high-frequency and ultrahigh-frequency discharges, Sov. Phys. Dokl. vol. 23 (1978) 44.
[8] W. Bongers, et al., Plasma-driven dissociation of CO_2 for fuel synthesis, Plasma Process. Polym. (2016), https://doi.org/10.1002/ppap.201600126.
[9] E.R. Mercer, et al., Post-plasma quenching to improve conversion and energy efficiency in a CO_2 microwave plasma, Fuel vol. 334 (2023) 126734, https://doi.org/10.1016/j.fuel.2022.126734.
[10] A.J. Wolf, T.W.H. Righart, F.J.J. Peeters, W.A. Bongers, M.C.M. van de Sanden, Implications of thermo-chemical instability on the contracted modes in CO_2 microwave plasmas, Plasma Sources Sci. Technol. vol. 29 (2) (2020) 25005, https://doi.org/10.1088/1361-6595/ab5eca.
[11] P. Viegas *et al.*, Insight into contraction dynamics of microwave plasmas for CO2 conversion, 2020.
[12] A. Van De Steeg, P. Viegas, A. Silva, T. Butterworth, A. Van Bavel, and J. Smits, Redefining the Microwave Plasma Mediated CO 2 Reduction Efficiency Limit: The role of O-CO2 Association, pp. 1–15.
[13] R.R. Wheeler, N.M. Hadley, S.R. Wambolt, J.T. Holtsnider, and R. Dewberry, Plasma Extraction of Oxygen from Martian Atmosphere, *45th International Conference on Environmental Systems*, no. July, pp. 1–12, 2015.
[14] G.J.C. Raposo, Plasma in-situ production of fuel and oxygen on Mars, Técnico Lisboa, 2020.
[15] V. Guerra, et al., Plasmas for in situ resource utilization on Mars: fuels, life support, and agriculture, J. Appl. Phys. vol. 132 (7) (2022) 70902, https://doi.org/10.1063/5.0098011.
[16] A.J. Wolf, T.W.H. Righart, F.J.J. Peeters, W.A. Bongers, M.C.M. Van De Sanden, Implications of thermo-chemical instability on the contracted modes in CO_2 microwave plasmas, Plasma Sources Sci. Technol. vol. 29 (2) (2020) 25005, https://doi.org/10.1088/1361-6595/ab5eca.
[17] S. Kelly, A. Bogaerts, Nitrogen fixation in an electrode-free microwave plasma, Joule vol. 5 (11) (2021) 3006–3030, https://doi.org/10.1016/j.joule.2021.09.009.
[18] S. Kelly, E. Mercer, R. De Meyer, R.-G. Ciocarlan, S. Bals, A. Bogaerts, Microwave plasma-based dry reforming of methane: Reaction performance and carbon formation, J. CO_2 Util. vol. 75 (2023) 102564, https://doi.org/10.1016/j.jcou.2023.102564.
[19] B. Wanten, R. Vertongen, R. De Meyer, A. Bogaerts, Plasma-based CO_2 conversion: how to correctly analyze the performance? J. Energy Chem. (2023) https://doi.org/10.1016/j.jechem.2023.07.005.
[20] S. Kelly, A. van de Steeg, A. Hughes, G. van Rooij, A. Bogaerts, Thermal instability and volume contraction in a pulsed microwave N2 plasma at sub-atmospheric pressure, Plasma Sources Sci. Technol. vol. 30 (5) (2021) 55005, https://doi.org/10.1088/1361-6595/abf1d6.
[21] S. Van Alphen, V. Vermeiren, T. Butterworth, D.C.M. van den Bekerom, G.J. van Rooij, A. Bogaerts, Power pulsing to maximize vibrational excitation efficiency in n2 microwave plasma: a combined experimental and computational study, J. Phys. Chem. C. vol. 124 (3) (. 2020) 1765–1779, https://doi.org/10.1021/acs.jpcc.9b06053.
[22] A.J. Wolf, T.W.H. Righart, F.J.J. Peeters, P.W.C. Groen, M.C.M. Van De Sanden, W. A. Bongers, Characterization of CO_2 microwave plasma based on the phenomenon of skin-depth-limited contraction, Plasma Sources Sci. Technol. vol. 28 (11) (2019), https://doi.org/10.1088/1361-6595/ab4e61.
[23] A. Berthelot, A. Bogaerts, Modeling of CO_2 splitting in a microwave plasma: how to improve the conversion and energy efficiency, J. Phys. Chem. C. vol. 121 (15) (2017) 8236–8251, https://doi.org/10.1021/acs.jpcc.6b12840.
[24] H. Schlüter, A. Shivarova, Travelling-wave-sustained discharges, Phys. Rep. vol. 443 (4–6) (2007) 121–255, https://doi.org/10.1016/j.physrep.2006.12.006.
[25] S. Heijkers, et al., CO_2 Conversion in a microwave plasma reactor in the presence of N2: elucidating the role of vibrational levels, J. Phys. Chem. C. vol. 119 (23) (. 2015) 12815–12828, https://doi.org/10.1021/acs.jpcc.5b01466.
[26] M. Ramakers, S. Heijkers, T. Tytgat, S. Lenaerts, A. Bogaerts, Combining CO_2 conversion and N2 fixation in a gliding arc plasmatron, J. CO_2 Util. vol. 33 (2019) 121–130, https://doi.org/10.1016/j.jcou.2019.05.015.
[27] W.Van Gaens, A. Bogaerts, Kinetic modelling for an atmospheric pressure argon plasma jet in humid air, J. Phys. D. Appl. Phys. vol. 46 (27) (2013) 275201, https://doi.org/10.1088/0022-3727/46/27/275201.

[28] G.J.M. Hagelaar, L.C. Pitchford, Solving the Boltzmann equation to obtain electron transport coefficients and rate coefficients for fluid models, Plasma Sources Sci. Technol. vol. 14 (4) (2005) 722, https://doi.org/10.1088/0963-0252/14/4/011.

[29] W. Wang, B. Patil, S. Heijkers, V. Hessel, A. Bogaerts, Nitrogen fixation by gliding arc plasma: better insight by chemical kinetics modelling, ChemSusChem vol. 10 (10) (2017) 2145–2157, https://doi.org/10.1002/cssc.201700095.

[30] B.S. Patil, J. Rovira Palau, V. Hessel, J. Lang, Q. Wang, Plasma nitrogen oxides synthesis in a milli-scale gliding arc reactor: investigating the electrical and process parameters, Plasma Chem. Plasma Process. vol. 36 (1) (2016) 241–257, https://doi.org/10.1007/s11090-015-9671-4.

[31] J. Zeldovich, The oxidation of nitrogen in combustion and explosions, Eur. Phys. J. A. Hadrons Nucl. vol. 21 (1946) 577–628.

[32] A. Bogaerts, E.C. Neyts, Plasma technology: an emerging technology for energy storage, ACS Energy Lett. vol. 3 (4) (2018) 1013–1027, https://doi.org/10.1021/acsenergylett.8b00184.

[33] T. Kozák, A. Bogaerts, Evaluation of the energy efficiency of CO_2 conversion in microwave discharges using a reaction kinetics model, Plasma Sources Sci. Technol. vol. 24 (1) (2015) 15024, https://doi.org/10.1088/0963-0252/24/1/015024.

[34] V. Guerra, et al., The case for in situ resource utilisation for oxygen production on Mars by non-equilibrium plasmas, Plasma Sources Sci. Technol. vol. 26 (11) (2017) 11LT01, https://doi.org/10.1088/1361-6595/aa8dcc.

[35] Mars Architecture Steering Group, Human Exploration of Mars Design Reference Architecture 5.0, Houston, Texas, 2009. doi:10.32964/tj8.7.

[36] J. Gruenwald, Human outposts on Mars: engineering and scientific lessons learned from history, CEAS Space J. vol. 6 (2) (2014) 73–77, https://doi.org/10.1007/s12567-014-0059-8.

[37] A. Conley, Jordan; Leflet, Devon; Shaw, Steve; Marchese, A Comparison of Preliminary Design Concepts for Liquid, Solid and Hybrid Propelled Mars Ascent Vehicles Using In-Situ Propellants." Accessed: Mar. 10, 2023. [Online]. Available: ⟨https://www.lpi.usra.edu/lpi/HEDS-UP/Rowan.pdf⟩.

[38] E. RONCACE, In-situ propellant rocket engines for Mars missions ascent vehicle, 1991, ⟨doi:10.2514/6.1991–2445⟩.

[39] J.C. Stern, et al., Evidence for indigenous nitrogen in sedimentary and aeolian deposits from the Curiosity rover investigations at Gale crater, Mars, Proc. Natl. Acad. Sci. vol. 112 (14) (2015) 4245–4250, https://doi.org/10.1073/pnas.1420932112.

[40] P. Kasiviswanathan, E.D. Swanner, L.J. Halverson, P. Vijayapalani, Farming on Mars: treatment of basaltic regolith soil and briny water simulants sustains plant growth (August), PLoS One vol. 17 (8) (2022) 1–16, https://doi.org/10.1371/journal.pone.0272209.

[41] B. Roberto and M. Candanosa, Fertilizing Mars, no. May, pp. 5–7, 2017.

[42] A.F. Davila, D. Willson, J.D. Coates, C.P. McKay, Perchlorate on Mars: a chemical hazard and a resource for humans, Int. J. Astro vol. 12 (4) (2013) 321–325, https://doi.org/10.1017/S1473550413000189.

[43] J. Wadsworth, C.S. Cockell, Perchlorates on Mars enhance the bacteriocidal effects of UV light, Sci. Rep. vol. 7 (1) (2017) 1–8, https://doi.org/10.1038/s41598-017-04910-3.

[44] J, Heinz, et al., Perchlorate-specific proteomic stress responses of Debaryomyces hansenii could enable microbial survival in Martian brines, Environ. Microbiol vol. 24 (11) (2022) 5051–5065, https://doi.org/10.1111/1462-2920.16152.

[45] F. Raganati, F. Miccio, P. Ammendola, Adsorption of carbon dioxide for post-combustion capture: a review, Energy Fuels vol. 35 (16) (2021) 12845–12868, https://doi.org/10.1021/acs.energyfuels.1c01618.

[46] W. Liu, et al., Steam-assisted temperature swing adsorption for carbon capture integrated with heat pump, Case Stud. Therm. Eng. vol. 49 (2023) 103233, https://doi.org/10.1016/j.csite.2023.103233.

[47] I.A.A.C. Esteves, J.P.B. Mota, Simulation of a new hybrid membrane/pressure swing adsorption process for gas separation, Desalination vol. 148 (1) (2002) 275–280, https://doi.org/10.1016/S0011-9164(02)00713-0.

[48] L. qun Zhu, J. ling Tu, Y. jun Shi, Separation of COCO2N2 gas mixture for high-purity CO by pressure swing adsorption, Gas. Sep. Purif. vol. 5 (3) (1991) 173–176, https://doi.org/10.1016/0950-4214(91)80015-W.

[49] I. Durán, F. Rubiera, C. Pevida, Vacuum swing CO_2 adsorption cycles in Waste-to-Energy plants, Chem. Eng. J. vol. 382 (2020) 1–32, https://doi.org/10.1016/j.cej.2019.122841.

[50] J.W. Yoon, et al., Highly selective adsorption of CO over CO_2 in a Cu(I)-chelated porous organic polymer, J. Hazard Mater. vol. 341 (2018) 321–327, https://doi.org/10.1016/j.jhazmat.2017.07.065.

[51] S. Kolbadinejad, H. Mashhadimoslem, A. Ghaemi, M. Bastos-Neto, Deep learning analysis of Ar, Xe, Kr, and O2 adsorption on activated carbon and zeolites using ANN approach, Chem. Eng. Process. - Process. Intensif. vol. 170 (September 2021) (2022) 108662, https://doi.org/10.1016/j.cep.2021.108662.

[52] S. Baumann, J.M. Serra, M.P. Lobera, S. Escolástico, F. Schulze-Küppers, W. A. Meulenberg, Ultrahigh oxygen permeation flux through supported Ba0.5Sr0.5Co0.8Fe0.2O3-δ membranes, J. Memb. Sci. vol. 377 (1–2) (2011) 198–205, https://doi.org/10.1016/j.memsci.2011.04.050.

[53] G. Chen, et al., Roadmap for sustainable mixed ionic-electronic conducting membranes, Adv. Funct. Mater. vol. 32 (6) (2022), https://doi.org/10.1002/adfm.202105702.

[54] R. Schultz, Matthias; Pippardt, Ute; Kiesel, Lutz; Ritter, Katrin; Kriegel, Oxygen permeation of various archetypes of oxygen membranes based on BSCF, AIChE J. vol. 59 (4) (2012) 215–228, https://doi.org/10.1002/aic.

[55] J. Van Noyen, et al., Fabrication of perovskite capillary membranes for high temperature gas separation, Catal. Today vol. 193 (1) (2012) 172–178, https://doi.org/10.1016/j.cattod.2012.03.005.

[56] S. Engels, T. Markus, M. Modigell, L. Singheiser, Oxygen permeation and stability investigations on MIEC membrane materials under operating conditions for power plant processes, J. Memb. Sci. vol. 370 (1–2) (2011) 58–69, https://doi.org/10.1016/j.memsci.2010.12.021.

[57] M. Arnold, H. Wang, A. Feldhoff, Influence of CO_2 on the oxygen permeation performance and the microstructure of perovskite-type (Ba0.5Sr0.5)(Co0.8Fe0.2)O3-δ membranes, J. Memb. Sci. vol. 293 (1–2) (2007) 44–52, https://doi.org/10.1016/j.memsci.2007.01.032.

[58] H. Lamberts-Van Assche, G. Thomassen, T. Compernolle, The early-stage design of plasma for the conversion of CO_2 to chemicals: a prospective techno-economic assessment, J. CO_2 Util. vol. 64 (2022) 102156, https://doi.org/10.1016/j.jcou.2022.102156.

[59] G.J. van Rooij, H.N. Akse, W.A. Bongers, M.C.M. van de Sanden, Plasma for electrification of chemical industry: a case study on CO2reduction, Plasma Phys. Control Fusion vol. 60 (1) (2018) 14019, https://doi.org/10.1088/1361-6587/aa8f7d.

[60] V. Maiwald, D. Schubert, D. Quantius, P. Zabel, From space back to Earth: supporting sustainable development with spaceflight technologies, Sustain. Earth vol. 4 (1) (2021), https://doi.org/10.1186/s42055-021-00042-9.

[61] U.A.K. Betz, et al., Game changers in science and technology - now and beyond, Technol. Forecast Soc. Change vol. 193 (May) (2023) 122588, https://doi.org/10.1016/j.techfore.2023.122588.

[62] M. The National Academies of Sciences, Engineering, Plasma science: Enabling Technology, Sustainability, Security, and Exploration, 2021, https://doi.org/10.17226/25802.

[63] R. Snoeckx, A. Bogaerts, Plasma technology-a novel solution for CO_2 conversion? Chem. Soc. Rev. vol. 46 (19) (2017) 5805–5863, https://doi.org/10.1039/c6cs00066e.

[64] A. Bogaerts, G. Centi, Plasma Technology for CO_2 Conversion: a personal perspective on prospects and gaps, Front. Energy Res. (2020), https://doi.org/10.3389/fenrg.2020.00111.

[65] A. Bogaerts, X. Tu, G. Rooij, M.C.M. Sanden, Plasma-based CO_2 conversion, in, Transformations (2019) 585–634, https://doi.org/10.1515/9783110665147-028.

[66] K. Werner, RF Energy Systems: Realizing New Applications, Microwave Journal, p. 22, Dec. 2015. Accessed: Oct. 25, 2023. [Online]. Available: ⟨https://www.microwavejournal.com/articles/25583-rf-energy-systems-realizing-new-applications⟩.

[67] E.F. Brown, The next-generation consumer microwave oven: a review, J. Microw. Power Electromagn. Energy vol. 56 (2) (. 2022) 82–86, https://doi.org/10.1080/08327823.2022.2066772.

[68] T. Kroc, V. Yakovlev, C. Thangaraj, B. Chase, R. Dhuley, The need for further development of magnetrons as RF sources for HEP, Snowmass (2022).

[69] D. Premathilake, R.A. Outlaw, R.A. Quinlan, C.E. Byvik, Oxygen generation by carbon dioxide glow discharge and separation by permeation through ultrathin silver membranes, Earth Space Sci. vol. 6 (4) (2019) 557–564, https://doi.org/10.1029/2018EA000521.